Boosting the Electrocatalytic Conversion of Nitrogen to Ammonia on Metal-Phthalocyanine-based Two-Dimensional Conjugated Covalent Organic Frameworks

Zhong, H.; Wang, M.; Ghorbani Asl, M.; Zhang, J.; Hoang Ly, K.; Liao, Z.-Q.; Chen, G.; Wei, Y.; Biswal, B. P.; Zschech, E.; Weidinger, I. M.; Krasheninnikov, A.; Dong, R.; Feng, X.;

Originally published:

November 2021

Journal of the American Chemical Society 143(2021)47, 19992-20000

DOI: https://doi.org/10.1021/jacs.1c11158

Boosting the Electrocatalytic Conversion of Nitrogen to Ammonia on Metal-Phthalocyanine-based Two-Dimensional Conjugated Covalent Organic Frameworks

Haixia Zhong[†#], Mingchao Wang[†#], Mahdi Ghorbani-Asl[‡#], Jichao Zhang[§#], Khoa Hoang Ly[†#], Zhongquan Liao[//], Guangbo Chen[†], Yidan Wei[‡], Bishnu P. Biswal[▽], Ehrenfried Zschech[//], Inez M. Weidinger[†], Arkady V. Krasheninnikov[‡,⊥], Renhao Dong[†Δ]*, Xinliang Feng[†ξ]*

[†]*Center for Advancing Electronics Dresden (cfaed) & Department of Chemistry and Food Chemistry, Technische Universität Dresden, Mommsenstrasse 4, 01062 Dresden, Germany*

[‡]*Institute of Ion Beam Physics and Materials Research, Helmholtz-Zentrum Dresden-Rossendorf e.V., Bautzner Landstr. 400, 01328 Dresden, Germany*

[§]*Shanghai Synchrotron Radiation Facility, Zhangjiang Laboratory, Shanghai Advanced Research Institute, Chinese Academy of Sciences, 201204 Shanghai, China*

[//]*Fraunhofer Institute for Ceramic Technologies and Systems (IKTS), Maria-Reiche-Strasse 2, 01109 Dresden, Germany*

[▽]*School of Chemical Sciences National Institute of Science Education and Research (NISER) Jatni, Khurda, Bhubaneswar, 752050 Odisha, India*

[⊥]*Department of Applied Physics, Aalto University, P.O. Box 11100, 00076 Aalto, Finland*

[Δ]*Key Laboratory of Colloid and Interface Chemistry of the Ministry of Education, School of Chemistry and Chemical Engineering, Shandong University, Jinan, 250100, China*

[ξ]*Max Planck Institute of Microstructure Physics, 06120 Halle (Saale), Germany*

ABSTRACT: Electrochemical N_2 reduction reaction (NRR) under ambient conditions is attractive for the great potential in replacing the current Haber-Bosch process towards sustainable ammonia production. Metal-heteroatom-doped carbon-rich materials have emerged as the most promising electrocatalysts for NRR. However, simultaneously boosting their activity and selectivity toward NRR remains a grand challenge, while the principle for precisely tailoring the active sites has been elusive. Herein, we report the first case of crystalline two-dimensional conjugated covalent organic frameworks (2D *c*-COFs) incorporated with M-N_4-C centers as novel, defined and effective catalysts, and achieve a simultaneous enhancement in the activity and selectivity towards electrochemical NRR to yield ammonia. Such 2D *c*-COFs are synthesized based on metal-phthalocyanine (M = Fe, Co, Ni, Mn, Zn and Cu) and pyrene building blocks bonded by pyrazine linkages. Significantly, the 2D *c*-COF catalysts with Fe-N_4-C center exhibit higher ammonia yield rate (33.6 μg $h^{-1}mg^{-1}_{cat}$) and Faradaic efficiency (FE, 31.9 %) at -0.1 V *vs.* reversible hydrogen electrode than those with other M-N_4-C centers, making them among the best NRR electrocatalysts (yield rate >30 μg $h^{-1}mg^{-1}_{cat}$ and FE >30 %). In-situ X-ray absorption spectroscopy, Raman spectroelectrochemistry and theoretical calculations unveil that the Fe-N_4-C center acts as a catalytic site. It shows a unique electronic structure with localized electronic states at the Fermi level, allowing for higher N_2 affinity and stronger binding energy of N_2, enabling faster N_2 activation and NRR kinetics than other M-N_4-C centers. Our work opens the possibility of developing metal-nitrogen-doped carbon-rich 2D *c*-COFs as superior NRR electrocatalyst and provides an atomic understanding of the NRR process on M-N_x-C based electrocatalysts for the design of high-performance NRR catalysts.

INTRODUCTION

Electrochemical nitrogen reduction reaction (NRR), particularly in conjunction with renewable energy, is regarded as a promising and sustainable alternative to the current high temperature/pressure Harber-Bosch process for the production of ammonia under ambient conditions.[1-3] Despite the increasing interest, electrochemical NRR process suffers from extremely sluggish kinetics and low selectivity due to the high energy barriers of N_2 activation and the faster kinetics of the competing hydrogen evolution reaction (HER) in the similar potential ranges,[3] respectively. To overcome the above challenges, a wide range of electrocatalysts have been developed to accelerate the NRR while simultaneously suppressing the HER process.[4-6] Homogenous catalysts, such as transitional metal complexes, which possess uniform and defined active sites, tunable catalytic environment and maximum atomic utilization, have been investigated as highly active NRR electrocatalysts.[3, 7] However, their practical applications are hindered by their poor stability and recyclability. In contrast, heterogeneous metal-heteroatom-doped carbon-rich electrocatalysts are a more attractive alternative because of their high durability and recyclability, as well as their ease of integration into the electrode.[2-6, 8-10] Recent advances have shown that iron-nitrogen-doped carbon-

rich electrocatalysts (Fe-N_x-C) could display either high NRR selectivity with a Faradaic efficiency (FE) >56.5% (while the yield rate is less than 8 $\mu g\ h^{-1}mg^{-1}_{cat}$)[2] or high NRR activity with a yield rate over 60 $\mu g\ h^{-1}mg^{-1}_{cat}$ (while the FE is around 18%).[11] Nevertheless, the inhomogeneity and ambiguity of the catalytic structure of iron-nitrogen-doped carbon posed major challenges in synergistically improving their activity and selectivity toward high NRR efficiency. Moreover, their inherently less defined catalytic environment hinders the fundamental studies on the reaction mechanism.

Two-dimensional conjugated covalent organic frameworks (2D *c*-COFs), with high in-plane π-delocalization and weak out-of-plane π-π stacking,[12-15] are emerging as a new type of carbon-rich electrocatalysts due to their unique layer-stacked periodic architecture, large surface area, structural tailorability, and chemical stability, as well as well-defined molecular catalytic sites. 2D *c*-COFs electrocatalysts with highly abundant accessible active sites and intrinsic electrical conductivity (up to 10^{-3} S cm^{-1}),[14, 16] have demonstrated high performance in electrocatalytic water splitting, oxygen reduction, and carbon dioxide reduction.[12, 17-22] In this respect, we consider that 2D c-COFs containing M-N_x-C centers would be attractive electrocatalysts for NRR because: 1) the columnar structure with pore array and high surface area can provide a large fraction of readily active sites and sufficient mass transport; 2) the intrinsic electrical conductivity can be beneficial for high-efficiency electron transfer kinetics.

Herein, we present the first example of 2D *c*-COFs immobilized with M-N_x-C centers as definite and effective electrocatalysts for fast NRR kinetics. These 2D *c*-COFs (**MPc-pz**, M= Fe, Co, Ni, Mn, Zn and Cu) comprise metal-phthalocyanine (MPc) and pyrene units bonded by chemically stable pyrazine linkages. We achieve a simultaneous boosting in activity and selectivity toward electrochemical NRR to ammonia and unveil the impact of different metallic active components on the catalytic performances. Among different **MPc-pz** with M-N_4-C centers, the obtained **FePc-pz** exhibits the best performance with NH_3 yield rate (33.6 $\mu g\ h^{-1}mg^{-1}_{cat}$) and Faradaic efficiency (31.9 %) at -0.1 V *vs.* reversible hydrogen electrode (RHE), ranking among the best NRR catalysts (>30 $\mu g\ h^{-1}mg^{-1}_{cat}$ and >30 %). In-situ X-ray absorption, in-situ Raman spectroelectrochemistry and theoretical calculation disclose that the NRR activity of **FePc-pz** originates from the engineered Fe atoms in the framework. Compared with other metal atoms, the Fe atoms of Fe-N_4-C possess a unique electronic structure with localized electronic states at the Fermi level, resulting in higher N_2 affinity and stronger binding energy of N_2 on Fe-N_4-C, thus exhibiting lower energy barriers of the potential-determining step and faster overall NRR kinetics. Our work highlights the potential of metal-nitrogen-incorporated 2D *c*-COFs as powerful carbon-rich electrocatalysts for N_2-to-NH_3 conversion, and provides an atomic understanding of the NRR process at various M-N_4-C motifs, shedding light on the rational design of effective NRR electrocatalysts.

RESULTS AND DISCUSSION

Synthesis and characterization of MPc-pz catalysts. Figure 1a presents the synthesis of MPc-based pyrazine-linked **MPc-pz** 2D *c*-COF through the polycondensation of *tert*-butylpyrene-tetraone (^{t}Bu-PT) and ortho-diphenylmethanimine-substituted (–N=CPh_2) MPc. In a typical synthesis of **FePc-pz**, FePc monomer comprising 2,3,9,10,16,17,23,24-octa-substituted –N=CPh_2 groups (abbreviated as **FePc(N=CPh_2)$_8$**, Figure S1) and ^{t}Bu-PT with the molar ratio of 1:2 were employed in a solvothermal reaction. This reaction was performed with a mixed solution of 1-methyl-2-pyrrolidone/mesitylene/6M acetic acid aqueous solution (4:2:1, v/v/v) in a vacuum-sealed Schlenk tube at 165 °C for 5 days, which yielded crystalline black-green powder. Fourier transform infrared (FT-IR) spectroscopy in Figure 1b confirms the formation of pyrazine linkages in **FePc-pz** with the stretching vibrations of pyrazine at 1533, 1466, and 1363 cm^{-1}, as well as the disappearance of the vibrational bands related to the –N=CPh_2 groups and the keto units of the starting monomers.[23] The crystalline structure of **FePc-pz** was demonstrated from the intense diffraction peaks at 4.0°, 16.3° and 26.2° in the powder X-ray diffraction (PXRD) pattern (Figure 1c), which correspond to (100), (400) and (002) plane, respectively. The experimental PXRD pattern is in good agreement with the calculated AA serrated stacking geometry. With the same synthetic procedure, we also synthesized other **MPc-Pz** 2D *c*-COFs with different M-N_4-C centers including Co, Ni, Mn, Zn, and Cu, which was verified by PXRD (Figure S2) and scanning electron microscopy (SEM) measurements (Figure S3-7).

Regarding the formation of pyrazine-linkage, we employed a unique multi-step Schiff-base reaction including the hydrolysis reaction of Schiff-base (–N=CPh_2) to amine (–NH_2) and a following Schiff-base condensation of –NH_2 and ketone (details seen in Figure S8–10). This multi-step reaction procedure using the highly soluble and oxidatively stable –N=CPh_2 monomer[24] enables the homogenous polycondensation and slows down the polymerization rate during the transformation of one Schiff-base (–N=CPh_2) to another Schiff-base (pyrazine as the final linkage), thus achieving high crystallinity. As contrast, the direct Schiff-base reaction between ^{t}Bu-PT and iron 2,3,9,10,16,17,23,24-octaaminophthalocyanine (Figure S11) could barely provide crystalline **FePc-pz**. In addition, according to the Scherrer's equation, **CuPc-Pz** synthesized through the above multi-step reaction presented a slightly superior averaged crystal size (~8.5 nm) to that of **CuPc-pz** (~8.0 nm) obtained via direct Schiff-base condensation.[23]

To investigate the porosity of **FePc-pz**, low-pressure nitrogen adsorption measurements at 77.3 K were performed (Figure S12). The derived BET (Brunauer-Emmett-Teller) surface area was calculated to be 290 $m^2\ g^{-1}$. The pore size distribution curve confirms the presence of abundant micro-pores (1.78 nm) and meso-pores (2.51 and 3.79 nm) for **FePc-pz**, which is beneficial for sufficient mass transport during the catalytic process.[9, 18] Transmission electron microscopy (TEM) and SEM images show that the **FePc-pz** sample comprises of aggregated nanoparticles (Figure S13). Element mapping images (Figure S14) reveal a homogenous distribution of Fe, C and N over the **FePc-pz** sample. The Fe loading of **FePc-pz** was determined to be 4.15 % (Table S1), which is close with the theoretical content (4.32 %).

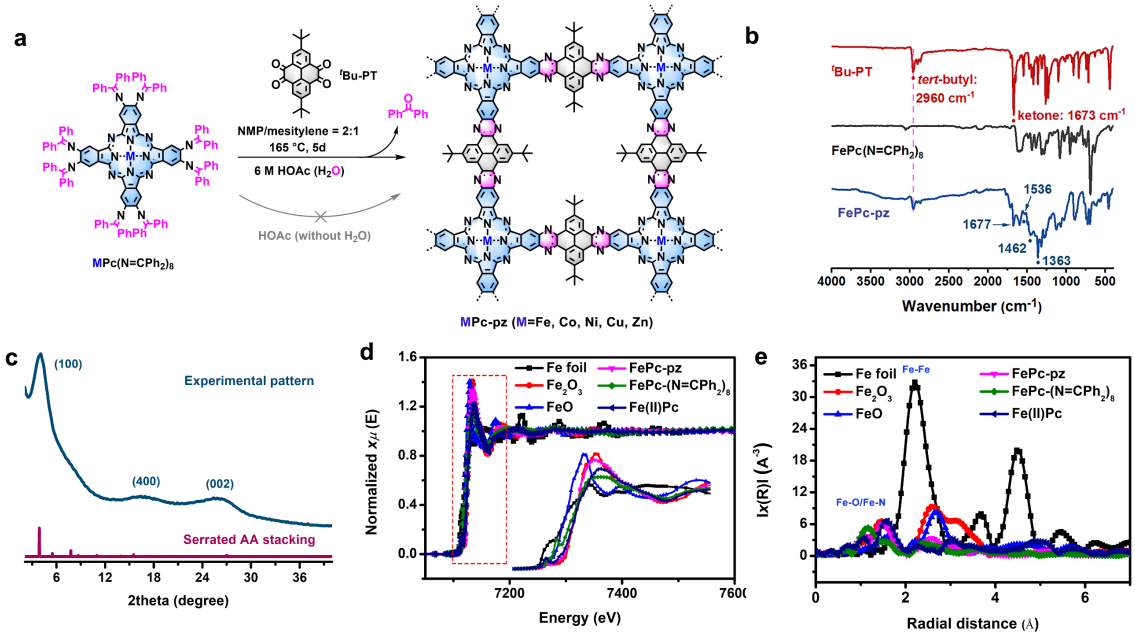

Figure 1. Structural characterization of **FePc-pz**. (a) Schematic synthesis process of **MPc-pz** (M=Fe, Co, Ni, Cu, Zn). (b) FT-IR spectra of Bu-PT, **FePc(N=CPh$_2$)$_8$** and **FePc-pz**. (c) Experimental and theoretical XRD pattern of **FePc-pz**. (d) Fe K-edge XANES spectra of Fe foil, FeO, Fe_2O_3, commercial iron (II) phthalocyanine (FePc), **FePc(N=CPh$_2$)$_8$** and **FePc-pz**. (e) Fourier transforms of Fe K-edge EXAFS spectra of Fe foil, FeO, Fe_2O_3, commercial Fe(II)Pc, **FePc(N=CPh$_2$)$_8$** and **FePc-pz**.

X-ray photoelectron spectroscopy (XPS, Figure S15) was conducted to study the composition and the chemical state of **FePc-pz**. The survey XPS spectrum also identifies the existence of Fe, C and N elements. In the fitted high-resolution N *1s* XPS spectra, the coordination peak of Fe and N is observed at 398.5 eV.[20] In the fitting Fe $2p_{3/2}$ XPS spectra, the dominant peak at 709.9 eV is assigned to Fe(II).[25-27] Additionally, XAS measurements (Figure 1d-e) were undertaken to analyse the oxidation state and coordination environment of Fe in **FePc-pz**. As shown in the Fe K-edge X-ray absorption near-edge structure (XANES) spectra (Figure 1d), **FePc-pz** displays a similar pre-edge peak (7113.8 eV) compared to the reference Fe(II)Pc (7113.6 eV), confirming the presence of FeN_4 centers in **FePc-pz**.[28] The difference in the pre-edge peaks of **FePc-pz** and Fe foil excludes the existence of metallic Fe species. Moreover, the main absorption peak of **FePc-pz** (7133.5 eV) located between FeO (7129.1 eV) and Fe_2O_3 (7140.2 eV) is also similar to Fe(II)Pc (7134.0 eV). It can be thus concluded that the oxidation valence of Fe atom is +2 in **FePc-pz**. The local structure of **FePc-pz** was analysed by the extended X-ray absorption fine structure (EXAFS) characterization. The characteristic Fe-N coordination signal appears at 1.53 Å (Figure 1e),[29] while the characteristic signal of Fe-Fe bonding at 2.21 Å is absent, which verifies the Fe-N coordination retained in the **FePc-pz** samples. **Electrochemical reduction of N_2 to NH_3.** The electrocatalytic NRR activity of **FePc-pz** was evaluated in a two-compartment electrochemical cell. A standard three-electrode system was used in 0.01 M H_2SO_4 electrolyte under ambient conditions, wherein the **FePc-pz** catalyst loaded on carbon paper (CP) was employed as the working electrode. In the linear scan voltammetry (LSV) curves (Figure S16a), an obvious increase of total current density (*j*) occurs in the potential range from 0.2 to -0.3 V *vs.* RHE when the electrolyte is saturated with N_2, indicative of a possible NRR process at the **FePc-pz** electrode. Subsequently, constant potential electrolysis of **FePc-pz** under different applied potentials was performed to analyse the generated products. Ammonia in the electrolyte was detected by the indophenol blue method using UV-Vis spectroscopy (Figure S17).[1, 30] The chronoamperometric results (Figure S16b) show that *j* of **FePc-pz** increases upon lowering the applied potential owing to the accelerated NRR and HER process. The NH_3 yield rate (YR) and Faradaic efficiency (FE) of **FePc-pz** follow a volcano-sharp trend with a summit value at -0.1 V vs RHE (**Figure 2a**-b). The rise of the competing HER becomes more favourable at higher overpotentials and hence progressively suppresses the NRR. At -0.1 V *vs.* RHE, the obtained YR and corresponding FE for NH_3 are up to 33.6 μg $h^{-1}mg^{-1}_{cat}$ and 31.9%, respectively, which are among the best reported NRR electrocatalysts (yield rate >30 μg $h^{-1}mg^{-1}_{cat}$ and FE >30%) (Figure 2a-b and Table S2). The current density in the CV curves, and FE and YR of ammonia for **FePc-pz** were similar when the electrolyte was kept with and without continuous stirring (Figure S18), suggesting that the mass transport is sufficient during the NRR process because of the porous structure of **FePc-pz**. Thus, NRR at **FePc-pz** electrode is a kinetics-controlled process rather than diffusion-controlled process. Next, nuclear magnetic resonance (NMR) analyses were employed to distinguish the triplet coupling of $^{14}NH_4^+$.[31, 32] Three peaks corresponding to $^{14}NH_4^+$ were found (Figure S19a) when supplying N_2 as feeding gas. In the control experiments, when using Ar-saturated electrolyte and bare CP electrode (Figure S19), no ammonia could be detected by UV-

vis and NMR measurements, confirming that NH_3 was generated exclusively from the electrocatalytic NRR on **FePc-pz**. Moreover, the signal of ammonium ion in the ion chromatography spectra further discloses the generation of ammonia via the electrolysis NRR process using **FePc-pz** electrode. (Figure S20). Additionally, N_2H_4 was not detected (Figure S21-22) in **FePc-pz** based electrocatalyst system via the Watt and Chrisp method. [28] In terms of stability, constant potential electrolysis was conducted at -0.1 V *vs.* RHE. Slight decline in YR (22.0 μg $h^{-1}mg^{-1}_{cat}$) and FE (23.6%) for the generated NH_3 was probed at the **FePc-pz** electrode after 4 cycles (Figure S23), which is likely due to partial peeling off of the catalyst from the current collector or the structural decomposition and passivation of the **FePc-pz**. As indicated by ex-situ SEM, Raman and FT-IR studies (Figure S24), the morphology and structure of **FePc-pz** remained after the NRR testing, ruling out the possibility of structural collapse of **FePc-pz** and generation of passivation film on the surface of **FePc-pz** electrode, and indicating the high stability of **FePc-pz** during the catalytic process, which were also confirmed by the following in-situ spectroscopy measurements (**Figure 3**). Besides, to alleviate the peeling-off of the active materials from the CP (Figure S23), in situ growth of **FePc-pz** on carbon paper can afford an improved stability with 86% reservation of current density, FE of 24.8% and ammonia yield rate of 27,5 μg $h^{-1}mg^{-1}_{cat}$ under 10 h continuous electrolysis, which is favorable for the practical application.

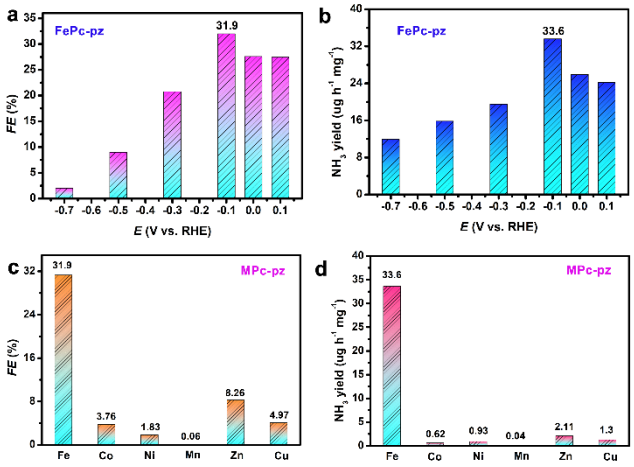

Figure 2. NRR performance. (a, b) Faradaic efficiency and NH_3 yield rate of **FePc-pz** under different electrolysis potentials in N_2-saturated 0.01 M H_2SO_4, respectively. (c, d) Faradaic efficiency and NH_3 yield rate of **MPc-pz** (M=Fe, Co, Ni, Mn, Cu, Zn) at -0.1 V *vs.* RHE in N_2-saturated 0.01 M H_2SO_4, respectively.

Contrast 2D *c*-COFs with different metal centers (**MPc-pz**, M=Co, Ni, Cu, Zn and Mn) were utilized to investigate the role of the metal center in NRR catalytic activity. As shown in Figure 2c-d, **FePc-pz** shows superior NRR performance in terms of yield rate and FE for NH_3 (33.6 μg $h^{-1}mg^{-1}_{cat}$ and 31.9 %), compared with **CoPc-pz** (3.76 μg $h^{-1}mg^{-1}_{cat}$ and 0.62 %), **NiPc-pz** (1.83 μg $h^{-1}mg^{-1}_{cat}$ and 0.93 %), **MnPc-pz** (0.06 μg $h^{-1}mg^{-1}_{cat}$ and 0.04 %), **ZnPc-pz** (8.26 μg $h^{-1}mg^{-1}_{cat}$ and 2.11 %) and **CuPc-pz** (4.97 μg $h^{-1}mg^{-1}_{cat}$ and 1.3 %) at -0.1 V *vs.* RHE. The control experiments demonstrate that the optimized M-N_4-C centers in 2D *c*-COFs play a key role in boosting the high NRR catalytic activity. Additionally, Figure S25 shows that the NRR catalytic activity of the commercial PcFe(+2) (YR: 4.32 μg $h^{-1}mg^{-1}_{cat}$; FE: 11.9%) and **FePc(N=CPh$_2$)$_8$** molecule (YR: 19.80 μg $h^{-1}mg^{-1}_{cat}$; FE: 17.9 %) are both lower than those of **FePc-pz** (Figure 2). further suggesting the advantages of **FePc-pz** 2D c-MOFs in promoting the NRR process.

Identification of the active sites of FePc-pz for NRR. In-situ XAS was employed to gain profound insight into the chemical state and coordination structure of Fe in the **FePc-pz** under NRR operating conditions (**Figure 3a-b**). The in-situ Fe K-edge XANES profiles of **FePc-pz** under different electrolysis potentials underline that no apparent change took place for **FePc-pz** samples during the NRR process. Notably, their pre-edge resonances appeared at 7113.7 eV due to electron transition from 4s to 4p when the applied potential was varied from open circuit voltage (OCV) to 0.1 V, -0.1 V and -0.3 V *vs.* RHE and finally back to the OCV. These pre-edge signals are similar with the ones of Fe(II)Pc but distinctly different from that of Fe foil, thus excluding the generation of metallic Fe species at **FePc-pz** electrodes during the NRR process.[28, 33, 34] Similarly, the main absorption peaks were found at 7133.5 eV for all the **FePc-pz** samples recorded under the NRR operation condition, elucidating that the oxidation state of Fe in **FePc-pz** remained +2 under this constant potential electrolysis condition, and excluding the oxidation of the Fe sites by possible surface adsorption of oxygen species or other impurities over the applied potential. Furthermore, Fe K-edge EXAFS oscillation analysis was applied to investigate the local coordination of the FeN_4 sites during the NRR process. As shown in Figure 3b, the characteristic peaks for Fe-N/O and Fe-Fe shell were respectively observed at 1.5 and 2.2 Å.[33, 35] By changing the applied potential from 0.1 to -0.3 V *vs.* RHE, this peak assigned to Fe-N shell of **FePc-pz** was shifted to 1.2 Å, indicating a compression of Fe-N coordination bond due to the interaction between the adsorbed N intermediates/hydrogen radicals and Fe sites during the NRR process.[33, 36, 37] Subsequently, the original Fe-N signals position at 1.5 Å was restored when the potentials were switched back to OCV, revealing no structural collapse in **FePc-pz** 2D c-COF. It is thus concluded that **FePc-pz** with active FeN_4 sites is a chemically and structurally stable NRR electrocatalyst.

In-situ Raman spectroelectrochemistry was applied to investigate the chemical structure of **FePc-pz** under NRR conditions. Laser excitation at 458 nm of **FePc-pz** hybridized with CNT yielded pre-resonance Raman spectra featuring a convolution of in-plane vibrations of the Pc unit and the linker.[38-41] Figure 3c shows the resonance Raman (RR) spectra of **FePc-pz** recorded under different conditions. A list of apparent bands and a tentative assignment based on comparison with the literature is presented in Table S3. In the dry state, the RR spectral pattern shares significant similarities with the literature results.[38, 39] Noteworthy, the relevant C_α-N_β-C_α bridge vibration of the Pc unit was supposedly found at 1538 cm^{-1}. This vibration occurs at significantly higher frequency compared to ordinary FePc where the respective band is located at ca. 1530 cm^{-1} or lower[38, 42, 43] implying a slightly distorted Pc ring in **FePc-pz** with the isoindol groups pulled towards the Fe atom.[42] This is supported by the smaller Fe-N distance of 1.5 Å determined by XAS (see above) compared with FePc molecules (1.53 Å). [38, 44] Interestingly, the decreased cavity size seems not to be directly associated with a relevant alteration of the Fe-N bond strength. This is concluded from the position of the 749 cm^{-1} band, assigned

to C_α-N_β-C_α bridge bending that is coupled to Fe-N stretching vibrations, which matches the frequency found for FePc molecules (750 cm^{-1}), suggesting a similar binding situation.[43, 45] Upon addition of 0.01 M H_2SO_4 solution and applying anodic potentials, *i.e.* > 0.2 V *vs.* RHE, no relevant spectral changes were observed (Figure 3c). Stepwise lowering the potential from 0.5 to -0.3 V *vs.* RHE in Ar and N_2 saturated electrolyte resulted in a reversible change of the spectral pattern after passing 0.1 V *vs.* RHE (Figure 3d, and Figure S26). The original spectral features of **FePc-pz** were replaced by a set of bands exhibiting significantly lowered Raman intensity,[1] while it could be restored when the potential was stepped back to 0.5 V *vs.* RHE (Figure 3d), suggesting a reversible event due to the adsorption/desorption of reactants/intermediates on these active unities. Component fit analysis was performed to extract the number and contributions of spectral components to the recorded RR spectra as a function of potential (Figure S27). The RR spectra could be satisfyingly reconstructed by a linear combination of two spectral components with varying factors. Plotting the normalized intensity of the component spectra against the potential yielded sigmoidal curve(s) (Figure S28). The obtained intensity trends match the results from cyclic voltammetry (Figure S16a, CV curves of **FePc-pz**), suggesting that the derived component spectra likely represent redox states of **FePc-pz**, designated as **FePc-pz**(O) and **FePc-pz**(R), which are stabilized above 0.4 V and below -0.1 V *vs.* RHE, respectively. In this respect, the altered band pattern showing peaks at 1302 cm^{-1}, 1334 cm^{-1}, 1416 cm^{-1}, 1445 cm^{-1}, 1505 cm^{-1}, and 1579 cm^{-1} may indicate a redox-induced structural change occurring at the Pc unit. Specifically, the observed bands match in-plane vibrations characteristic for Pc structures accommodating large metal ions that afford an increase of the Pc pocket.[38] As such, the potential-dependent Raman data could be rationalized by a redox event at the Fe as a result of applying cathodic potentials. The increased ion size would lead to a reduced Fe-N distance and an expansion of the Pc cavity, which give rise to the altered Raman spectral pattern. This is corroborated by XAS measurements that a decrease in Fe-N distance was observed from 1.5 to 1.2 Å at 0.1 and -0.3 V vs. RHE, respectively. Though such phenomenon is usually observed only for much larger cations, such as Pb^{2+} the unusually small Pc ring size of 3 Å (N-Fe-N distance) could facilitate the structural impact of the increased Fe shell due to the interaction of the reactants/intermediates upon the applied potentials.[38, 42]

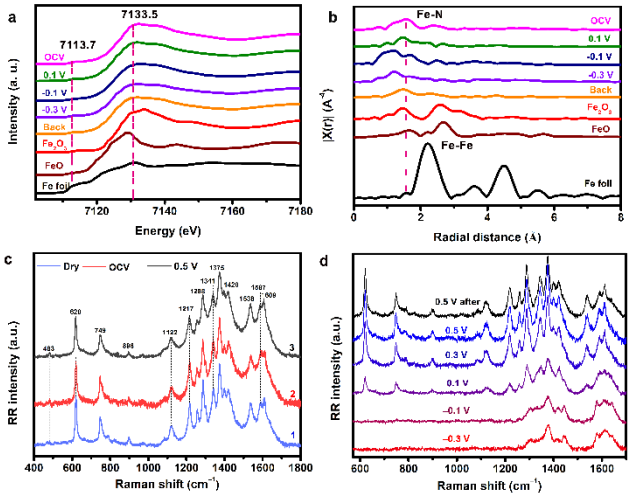

Figure 3. *In-situ* XAS and Raman measurement under electrolysis. (a, b) Fe k-edge XANES and EXAFS profiles of Fe foil, FeO, Fe_2O_3, **FePc-pz** on carbon paper under different applied potential (OCV, 0.1, -0.1, -0.3 V *vs.* RHE, back to OCV), respectively. (c) Resonance Raman spectra of the **FePc-pz** electrode excited as 458 nm and recorded at three different experimental conditions (dry; at OCV in Ar saturated 0.01 M H_2SO_4; at 0.5 V *vs.* RHE). (d) Potential-dependent resonance Raman spectra of **FePc-pz** electrode in N_2 saturated 0.01 M H_2SO_4.

Electronic structure and NRR pathways investigation. Density functional theory (DFT) calculations were conducted to model the NRR reaction process on **MPc-pz** (Figure S29 and Table S4). An associative mechanism was considered in this catalyst system due to the extremely high activation energy of N_2 along with dissociative process (detail elementary steps seen in Supplementary methods).[46, 47]. The adsorption of NH_x and N_2H_x (x=0, 1, 2) molecules on **MPc-pz** (M: Mn, Fe, Co, Ni, Cu, Zn) were further investigated and the results are presented in Table S5. By comparing the calculated adsorption energies of N_2 at different positions in **MPc-pz**, the MN_4 centres are the most catalytically active sites for the electrocatalytic NRR process (Figure S30). The adsorption of N_2 on lattice nitrogen is less favorable (0.12 eV-0.14 eV) as compared to the adsorption on top of the metal center (Table S5). This means that NRR process of **MPc-pz**, is unlikely on lattice nitrogen, which is associated with the electronic properties of the metal atoms of **MPc-pz.** The charge density difference of **MPc-pz** with N_2 adsorbed on M-N_4-C centres reveals that a positive charge mainly locates around the metal atom, which plays an important role in polarizing and activating N_2 molecules (Figure 4a and Figure S31). Thereby, Co-N_4-C and Fe-N_4-C are found to be more susceptible for the reaction with molecular N_2, affording higher adsorption energies of N_2 on the Co (-0.35 eV) and Fe sites (-0.29 eV) than other contrast metal centers (Table S5; Cu: -0.28 eV; Mn: -0.16 eV; Ni: -0.07 eV; Zn: -0.10 eV).[11, 47, 48] Bader charge analysis (Table S6) shows that the amounts of transferred charges from Co (0.27 e) and Fe (0.26 e) to N_2 molecule are significantly larger than those of the other metals (Ni, 0.03 e; Cu, 0.02 e; Zn, 0.03 e; Mn, 0.12 e), which further explains the stronger interaction between Fe/Co and N_2 molecule. It was also found that the M-N bond length between the adsorbed N_2 and M atom was shortest for **FePc-pz** (2.09 Å) and **CoPc-pz** (2.02 Å) among all the M-N_4-C active sites (Table S7; Cu: 3.32 Å; Mn: 2.33 Å; Zn: 2.76 Å; Ni, 3.00 Å), while the average M-N bond length change in their M-N_4-C centres was the largest due to the uplift heights of Fe and Co atoms (Table S8). This is because of π-back bonding of the d electron from the M atom to the π* antibonding orbitals of N_2. In addition, the M-N bond strength of M-N_4-C sites is dramatically decreased by the electron-filled antibonding orbital, resulting in a longer M-N bond.[49] Therefore, **FePc-pz** and **CoPc-Pz** demonstrate the higher affinity of N_2 and favourable N_2 activation process.

The electronic structures of **MPc-pz** 2D *c*-COFs have been further calculated in the presence of N_2 molecule. The projected density of states (PDOS) for **FePc-pz** and **MnPc-pz** demonstrate the localized electronic states at the Fermi level, originating mainly from *d* orbitals of metal atoms (Figure 4b and Figure S32). In addition, the states from the N_2 molecule hybridize with Fe and Mn orbitals near the Fermi energy level (Figure 4c and Figure S33), while no interaction was observed for the other metals, revealing stronger binding energies of N_2 on Fe-N_4-C and Mn-N_4-C sites. As a consequence, **FePc-pz** theoretically exhibits superior NRR performance to the other MN_4-based COF electrocatalysts.

Next, NRR process of **MPc-pz** was investigated by computing the free energies of each elementary step in both the distal and alternating pathways (Figure 4d-e and Figure S34). The results of **MPc-pz** (Figure S35) suggest that the energy barrier of forming *H on **CoPc-pz** is smaller than that on **FePc-pz**, corresponding to a faster HER kinetics (Table S9-10). As a result, even though **CoPc-pz** also shows the potential toward NRR, the strong competition from HER greatly suppresses the NRR process on Co-N_4-C sites and results in low FE and yield rate of NH_3 for **CoPc-pz**. Therefore, the free energy profiles further confirm that **FePc-pz** containing Fe-N_4-C active unit is more effective for electrocatalytic NRR than other MN_4-based COF catalysts.

CONCLUSION

In summary, we have demonstrated the pyrazine-linked metal-phthalocyanine (MPc)-based 2D *c*-COFs (M=Fe, Co, Ni, Mn, Zn and Cu) as efficient electrocatalysts for simultaneously enhancing NRR activity and selectivity in acidic electrolyte and

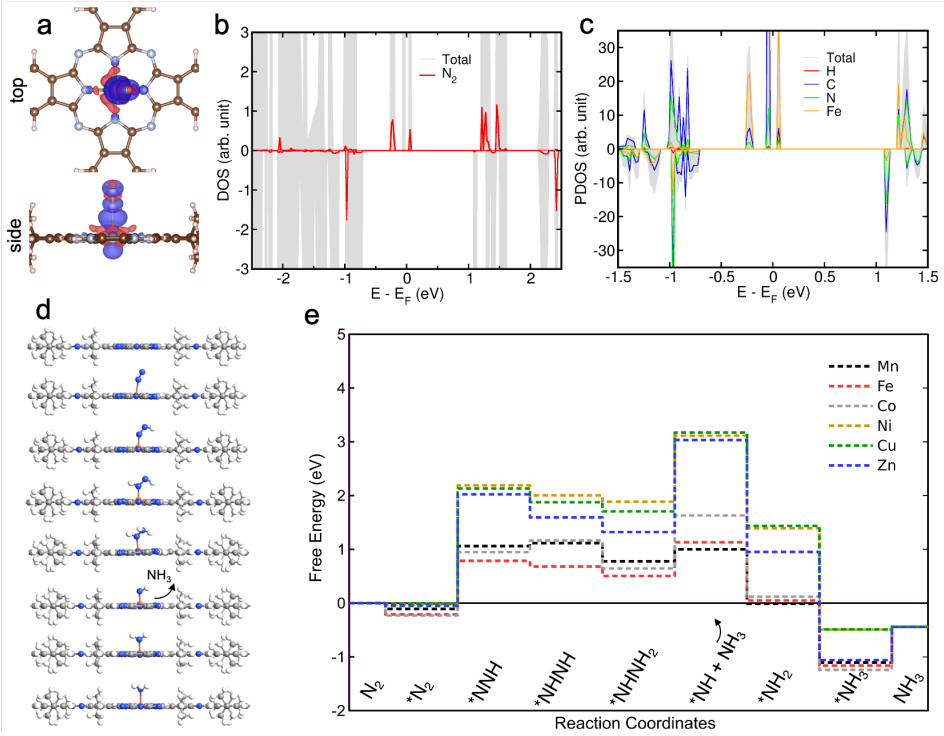

Figure 4. DFT calculation of NRR on **MPc-pz** 2D *c*-COFs (M=Fe, Co, Ni, Cu, Zn and Mn). (a) Charge density differences of N_2 adsorbed on **FePc-pz** as compared to the isolated N_2 molecule and **MPc-pz**. (b) Projected density of states (PDOS) for the most stable N_2 adsorption configuration on **MPc-pz** with MN_4. (c) DOS of **FePc-pz**. Red colors indicate partial projections on the N_2 molecule. (d) Optimized structures of various intermediates for NRR reaction. (e) Free energy profiles of NRR along the alternating pathway on **MPc-pz** (M: Mn, Fe, Co, Ni, Cu, Zn).

show that the rate determining step (RDS) of **MPc-pz** is the protonation of adsorbed N_2 to form *NNH, which is in line with its high activity toward NRR process. Besides, the alternating hydrogenation to form *NHNH is more energetically favourable than the distal hydrogenation to form *NNH_2 on **FePc-pz**. A high barrier energy has to be paid by the reduction of *NNH_2 to *N and NH_3, while the hydrogenation of *NHNH to *$NHNH_2$ releases energy. As a result, NRR tends to undergo the alternating pathway rather than the distal pathway on **FePc-pz**. In addition, the free energy profiles of HER on M-N_4-C sites elucidated the essential role of the metal active centers in controlling the catalytic performance. Thanks to the columnar stacking of porous array, high in-plane π-conjugation with fast electron transfer and plenty of Fe-N_4-C sites, the **FePc-pz** exhibited excellent catalytic performance with NH_3 yield rate of 33.6 μg $h^{-1}mg^{-1}_{cat}$ and Faradaic efficiency of 31.9 % at -0.1 V *vs.* RHE. In-situ XAS and Raman spectroelectrochemistry analyses, theoretical calculation and well-designed contrast electrochemical tests unveiled the unique properties of the FeN_4 active sites for N_2 activation and conversion by exhibiting an optimal

substrate adsorption energy as well as a low energy barrier for the RDS. Our work sheds light on the development of carbon-rich electrocatalysts with suitable M-N_x-C active sites for NRR, and contributes to a solid understanding on the origin of NRR activity, thus spotlighting the view on the rational design of high-performance molecular-like heterogeneous NRR electrocatalysts.

ASSOCIATED CONTENT

Supporting Information

The Supporting Information is available free of charge on the ACS Publications website. Synthetic details, characterization, theoretical calculation and electrochemical tests. (PDF).

AUTHOR INFORMATION

Corresponding Author

Renhao Dong − Center for Advancing Electronics Dresden and Department of Chemistry and Food Chemistry, Technische Universität Dresden, 01062 Dresden, Germany; Key Laboratory of Colloid and Interface Chemistry of the Ministry of Education, School of Chemistry and Chemical Engineering, Shandong University, Jinan, 250100, China. http://orcid.org/0000-0002-4125-9284; Email: **renhao.dong@tu-dresden.de**

Xinliang Feng − Center for Advancing Electronics Dresden and Department of Chemistry and Food Chemistry, Technische Universität Dresden, 01062 Dresden, Germany; Max Planck Institute of Microstructure Physics, Halle (Saale) 06120, Germany; http://orcid.org/0000-0003-3885-2703; Email: **xinliang.feng@tu-dresden.de**

Authors

Haixia Zhong − Center for Advancing Electronics Dresden and Department of Chemistry and Food Chemistry, Technische Universität Dresden, 01062 Dresden, Germany; http://orcid.org/0000-0002-2839-0253

Mingchao Wang − Center for Advancing Electronics Dresden and Department of Chemistry and Food Chemistry, Technische Universität Dresden, 01062 Dresden, Germany; https://orcid.org/0000-0001-9979-3503

Mahdi Ghorbani-Asl − Helmholtz-Zentrum Dresden-Rossendorf e.V., Institute of Ion Beam Physics and Materials Research, 01328 Dresden, Germany; https://orcid.org/0000-0003-3060-4369

Jichao Zhang− 3Shanghai Synchrotron Radiation Facility, Zhangjiang Laboratory, Shanghai Advanced Research Institute, Chinese Academy of Sciences, 201204 Shanghai, China; https://orcid.org/0000-0002-7400-6726

Khoa Hoang Ly − Center for Advancing Electronics Dresden and Department of Chemistry and Food Chemistry, Technische Universität Dresden, 01062 Dresden, Germany; https://orcid.org/0000-0003-4458-432X

Zhongquan Liao − Fraunhofer Institute for Ceramic Technologies and Systems (IKTS), Maria-Reiche-Strasse 2, 01109 Dresden, Germany; https://orcid.org/0000-0001-7868-4594

Guangbo Chen − Center for Advancing Electronics Dresden and Department of Chemistry and Food Chemistry, Technische Universität Dresden, 01062 Dresden, Germany; https://orcid.org/0000-0003-1927-3642

Bishnu P. Biswal − School of Chemical Sciences National Institute of Science Education and Research (NISER) Jatni, Khurda, Bhubaneswar, 752050 Odisha, India; https://orcid.org/0000-0002-8565-4550

Ehrenfried Zschech − Fraunhofer Institute for Ceramic Technologies and Systems (IKTS), Maria-Reiche-Strasse 2, 01109 Dresden, German; https://orcid.org/0000-0002-5220-3083

Inez M. Weidinger − Center for Advancing Electronics Dresden and Department of Chemistry and Food Chemistry, Technische Universität Dresden, 01062 Dresden, Germany; https://orcid.org/0000-0001-9316-6349

Arkady V. Krasheninnikov − Helmholtz-Zentrum Dresden-Rossendorf e.V., Institute of Ion Beam Physics and Materials Research, 01328, Dresden, Germany, Department of Applied Physics, Aalto University, P.O. Box 11100, 00076 Aalto, Finland; https://orcid.org/0000-0003-0074-7588

Author Contributions

The manuscript was written through contributions of all authors. [#]These authors contributed equally.

Notes

The authors declare no competing interests.

ACKNOWLEDGMENT

This work is financially supported by EU Graphene Flagship (GrapheneCore3, No. 881603), ERC starting grant (FC2DMOF, No. 852909), ERC Consolidator Grant (T2DCP), Coordination Networks: Building Blocks for Functional Systems (SPP 1928, COORNET), and CRC 1415 (Chemistry of Synthetic Two-Dimensional Materials, No. 417590517), as well as the German Science Council and Center for Advancing Electronics Dresden (cfaed). R.D. thanks Taishan Scholars Program of Shandong Province (tsqn201909047). H.Z. gratefully acknowledges funding from the Alexander von Humboldt Foundation. I.M.W. acknowledges the Cluster of Excellence UniSysCat (EXC 2008/1-390540038). We acknowledge Dresden Center for Nanoanalysis (DCN) at TUD and Dr. Petr Formanek (Leibniz Institute for Polymer Research, IPF, Dresden) for the use of facilities. We thank the scientists at beamline BL14W1 and BL15U1 of the Shanghai Synchrotron Radiation Facility for the XAFS measurements. We appreciate Prof. Thomas Heine and Hung-Hsuan Lin for providing the structural model. We also appreciate Na Zhou for IC measurement from Changchun institute of applied chemistry (CIAC). We thank Prof. Xiaodong Zhuang for the in-situ XAS electrochemical cell setup. The computational support from the HZDR computing cluster, Technical University of Dresden cluster (TAURUS), from High Performance Computing Center (HLRS) in Stuttgart, Germany, and CSC Finland, is gratefully appreciated.

REFERENCES

(1) Wang, J.; Yu, L.; Hu, L.; Chen, G.; Xin, H.; Feng, X., Ambient ammonia synthesis via palladium-catalyzed electrohydrogenation of dinitrogen at low overpotential. *Nat. Commun.* **2018,** *9* (1), 1795.

(2) Wang, M.; Liu, S.; Qian, T.; Liu, J.; Zhou, J.; Ji, H.; Xiong, J.; Zhong, J.; Yan, C., Over 56.55% faradaic efficiency of ambient ammonia synthesis enabled by positively shifting the reaction potential. *Nat. Commun.* **2019,** *10* (1), 341.

(3) Qing, G.; Ghazfar, R.; Jackowski, S. T.; Habibzadeh, F.; Ashtiani, M. M.; Chen, C. P.; Smith, M. R., 3rd; Hamann, T. W., Recent advances and challenges of electrocatalytic N_2 reduction to ammonia. *Chem. Rev.* **2020,** *120* (12), 5437–5516.

(4) Zhao, S.; Lu, X.; Wang, L.; Gale, J.; Amal, R., Carbon-based metal-free catalysts for electrocatalytic reduction of nitrogen for synthesis of ammonia at ambient conditions. *Adv. Mater.* **2019,** *31* (13), e1805367.

(5) Liu, Y. T.; Chen, X.; Yu, J.; Ding, B., Carbon-nanoplated CoS@TiO_2 nanofibrous membrane: an interface-engineered heterojunction for high-

efficiency electrocatalytic nitrogen reduction. *Angew .Chem. Int. Ed.* **2019,** *58* (52), 18903-18907.
(6) Li, M.; Huang, H.; Low, J.; Gao, C.; Long, R.; Xiong, Y., Recent progress on electrocatalyst and photocatalyst design for nitrogen reduction. *Small Methods* **2018,** *3* (6), 1800388.
(7) He, C.; Wu, Z.-Y.; Zhao, L.; Ming, M.; Zhang, Y.; Yi, Y.; Hu, J.-S., Identification of FeN4 as an efficient active site for electrochemical N_2 reduction. *ACS Catal.* **2019,** *9* (8), 7311-7317.
(8) Zhang, J.; Chen, G.; Mullen, K.; Feng, X., Carbon-Rich Nanomaterials: Fascinating Hydrogen and Oxygen Electrocatalysts. *Adv. Mater.* **2018**, e1800528.
(9) Zhong, H.; Ly, K. H.; Wang, M.; Krupskaya, Y.; Han, X.; Zhang, J.; Zhang, J.; Kataev, V.; Büchner, B.; Weidinger, I. M.; Kaskel, S.; Liu, P.; Chen, M.; Dong, R.; Feng, X., A phthalocyanine-based Layered two-dimensional conjugated metal–organic framework as a highly efficient electrocatalyst for the oxygen reduction teaction. *Angew. Chem. Int. Ed.* **2019,** *58* (31), 10677-10682.
(10) Zhong, H.; Ghorbani-Asl, M.; Ly, K. H.; Zhang, J.; Ge, J.; Wang, M.; Liao, Z.; Makarov, D.; Zschech, E.; Brunner, E.; Weidinger, I. M.; Zhang, J.; Krasheninnikov, A. V.; Kaskel, S.; Dong, R.; Feng, X., Synergistic electroreduction of carbon dioxide to carbon monoxide on bimetallic layered conjugated metal-organic frameworks. *Nat. Commun.* **2020,** *11* (1), 1409.
(11) Lü, F.; Zhao, S.; Guo, R.; He, J.; Peng, X.; Bao, H.; Fu, J.; Han, L.; Qi, G.; Luo, J.; Tang, X.; Liu, X., Nitrogen-coordinated single Fe sites for efficient electrocatalytic N_2 fixation in neutral media. *Nano Energy* **2019,** *61*, 420-427.
(12) Lin, S.; Diercks, C. S.; Zhang, Y.-B.; Kornienko, N.; Nichols, E. M.; Zhao, Y.; Paris, A. R.; Kim, D.; Yang, P.; Yaghi, O. M.; Chang, C. J., Covalent organic frameworks comprising cobalt porphyrins for catalytic CO_2 reduction in water. *Science* **2015,** *349* (6253), 1208.
(13) Bi, S.; Yang, C.; Zhang, W.; Xu, J.; Liu, L.; Wu, D.; Wang, X.; Han, Y.; Liang, Q.; Zhang, F., Two-dimensional semiconducting covalent organic frameworks via condensation at arylmethyl carbon atoms. *Nat. Commun.* **2019,** *10* (1), 2467.
(14) Song, J.; Wei, C.; Huang, Z. F.; Liu, C.; Zeng, L.; Wang, X.; Xu, Z. J., A review on fundamentals for designing oxygen evolution electrocatalysts. *Chem. Soc. Rev.* **2020,** *49* (7), 2196-2214.
(15) Yu, M.; Chandrasekhar, N.; Raghupathy, R. K. M.; Ly, K. H.; Zhang, H.; Dmitrieva, E.; Liang, C.; Lu, X.; Kühne, T. D.; Mirhosseini, H.; Weidinger, I. M.; Feng, X., A high-tate two-fimensional polyarylimide covalent organic framework anode for aqueous Zn-ion energy storage eevices. *J. Am. Chem. Soc.* **2020,** *142* (46), 19570-19578.
(16) Lakshmi, V.; Liu, C.-H.; Rajeswara Rao, M.; Chen, Y.; Fang, Y.; Dadvand, A.; Hamzehpoor, E.; Sakai-Otsuka, Y.; Stein, R. S.; Perepichka, D. F., A two-dimensional poly(azatriangulene) covalent organic framework with semiconducting and paramagnetic states. *J. Am. Chem. Soc.* **2020,** *142* (5), 2155-2160.
(17) Wang, D.-G.; Qiu, T.; Guo, W.; Liang, Z.; Tabassum, H.; Xia, D.; Zou, R., Covalent organic framework-based materials for energy applications. *Energy Environ. Sci.* **2021,** *14* (2), 688-728.
(18) Zhao, X.; Pachfule, P.; Li, S.; Langenhahn, T.; Ye, M.; Schlesiger, C.; Praetz, S.; Schmidt, J.; Thomas, A., Macro/microporous covalentorganic frameworks for efficient electrocatalysis. *J. Am. Chem. Soc.* **2019,** *141* (16), 6623-6630.
(19) Dong, J.; Han, X.; Liu, Y.; Li, H.; Cui, Y., Metal–covalent organic frameworks (MCOFs): a bridge between metal–organic frameworks and covalent organic frameworks. *Angew. Chem. Int. Ed.* **2020,** *59* (33), 13722-13733.
(20) Guo, J.; Lin, C. Y.; Xia, Z.; Xiang, Z., A pyrolysis-free covalent organic polymer for oxygen reduction. *Angew. Chem. Int. Ed.* **2018,** *57* (38), 12567-12572.
(21) Yu, M.; Dong, R.; Feng, X., Two-dimensional carbon-rich conjugated frameworks for electrochemical energy applications. *J. Am. Chem. Soc.* **2020,** *142* (30), 12903-12915.
(22) Wang, M.; Dong, R.; Feng, X., Two-dimensional conjugated metal-organic frameworks (2D c-MOFs): chemistry and function for MOFtronics. *Chem. Soc. Rev.* **2021,** *50* (4), 2764-2793.
(23) Wang, M.; Ballabio, M.; Wang, M.; Lin, H. H.; Biswal, B. P.; Han, X.; Paasch, S.; Brunner, E.; Liu, P.; Chen, M.; Bonn, M.; Heine, T.; Zhou, S.; Canovas, E.; Dong, R.; Feng, X., Unveiling electronic properties in metal-phthalocyanine-based pyrazine-Linked conjugated two-dimensional covalent organic frameworks. *J. Am. Chem. Soc.* **2019,** *141* (42), 16810-16816.
(24) Vitaku, E.; Dichtel, W. R., Synthesis of 2D Imine-Linked Covalent Organic Frameworks through Formal Transimination Reactions. *J. Am. Chem. Soc.* **2017,** *139* (37), 12911-12914.
(25) Grosvenor, A. P.; Kobe, B. A.; Biesinger, M. C.; McIntyre, N. S., Investigation of multiplet splitting of Fe 2p XPS spectra and bonding in iron compounds. *Surf. Interface Anal.* **2004,** *36* (12), 1564-1574.
(26) Paparazzo, E., XPS and auger spectroscopy studies on mixtures of the oxides SiO_2, Al_2O_3, Fe_2O_3 and Cr_2O_3. *J Electron Spectros Relat Phenomena* **1987,** *43* (2), 97-112.
(27) Ivanova, T. M.; Linko, R. V.; Petrov, A. V.; Bazanov, M. I.; Dyumaev, K. M., Effect of the nature of axial ligand on the effective charge of the metal center in PcFe(II) complexes. *Russ. J. Inorg. Chem.* **2008,** *53* (11), 1784-1787.
(28) Gu, J.; Hsu, C.-S.; Bai, L.; Chen, H. M.; Hu, X., Atomically dispersed Fe^{3+} sites catalyze efficient CO_2 electroreduction to CO. *Science* **2019,** *364* (6445), 1091.
(29) Qiao, M.; Wang, Y.; Wang, Q.; Hu, G.; Mamat, X.; Zhang, S.; Wang, S., Hierarchically ordered porous carbon with atomically dispersed FeN_4 for ultraefficient oxygen reduction reaction in proton-exchange membrane fuel cells. *Angew. Chem. Int. Ed.* **2020,** *59* (7), 2688-2694.
(30) Searle, P. L., The berthelot or indophenol reaction and its use in the analytical chemistry of nitrogen. A review. *Analyst* **1984,** *109* (5), 549-568.
(31) Zhao, Y.; Shi, R.; Bian, X.; Zhou, C.; Zhao, Y.; Zhang, S.; Wu, F.; Waterhouse, G. I. N.; Wu, L. Z.; Tung, C. H.; Zhang, T., Ammonia detection methods in photocatalytic and electrocatalytic experiments: how to improve the reliability of NH_3 production rates? *Adv. Sci.* **2019,** *6* (8), 1802109.
(32) Luo, Y.; Chen, G.-F.; Ding, L.; Chen, X.; Ding, L.-X.; Wang, H., Efficient electrocatalytic N_2 fixation with MXene under ambient conditions. *Joule* **2019,** *3* (1), 279-289.
(33) Genovese, C.; Schuster, M. E.; Gibson, E. K.; Gianolio, D.; Posligua, V.; Grau-Crespo, R.; Cibin, G.; Wells, P. P.; Garai, D.; Solokha, V.; Krick Calderon, S.; Velasco-Velez, J. J.; Ampelli, C.; Perathoner, S.; Held, G.; Centi, G.; Arrigo, R., Operando spectroscopy study of the carbon dioxide electro-reduction by iron species on nitrogen-doped carbon. *Nat. Commun.* **2018,** *9* (1), 935.
(34) Zhang, Z.; Xiao, J.; Chen, X. J.; Yu, S.; Yu, L.; Si, R.; Wang, Y.; Wang, S.; Meng, X.; Wang, Y.; Tian, Z. Q.; Deng, D., Reaction mechanisms of well-defined metal-N_4 aites in electrocatalytic CO_2 reduction. *Angew. Chem. Int. Ed.* **2018,** *57* (50), 16339-16342.
(35) Wei, S.; Wang, Y.; Chen, W.; Li, Z.; Cheong, W.-C.; Zhang, Q.; Gong, Y.; Gu, L.; Chen, C.; Wang, D.; Peng, Q.; Li, Y., Atomically dispersed Fe atoms anchored on COF-derived N-doped carbon nanospheres as efficient multi-functional catalysts. *Chem. Sci.* **2020,** *11* (3), 786-790.
(36) Yang, H. B.; Hung, S.-F.; Liu, S.; Yuan, K.; Miao, S.; Zhang, L.; Huang, X.; Wang, H.-Y.; Cai, W.; Chen, R.; Gao, J.; Yang, X.; Chen, W.; Huang, Y.; Chen, H. M.; Li, C. M.; Zhang, T.; Liu, B., Atomically dispersed Ni(i) as the active site for electrochemical CO_2 reduction. *Nat. Energy* **2018,** *3* (2), 140-147.
(37) Cao, L.; Luo, Q.; Liu, W.; Lin, Y.; Liu, X.; Cao, Y.; Zhang, W.; Wu, Y.; Yang, J.; Yao, T.; Wei, S., Identification of single-atom active sites in carbon-based cobalt catalysts during electrocatalytic hydrogen evolution. *Nat. Catal.* **2018,** *2* (2), 134-141.
(38) Klyamer, D. D.; Basova, T. V.; Krasnov, P. O.; Sukhikh, A. S., Effect of fluorosubstitution and central metals on the molecular structure and vibrational spectra of metal phthalocyanines. *J. Mol. Struct.* **2019,** *1189*, 73-80.
(39) Szybowicz, M.; Makowiecki, J., Orientation study of iron phthalocyanine (FePc) thin films deposited on silicon substrate investigated by atomic force microscopy and micro-Raman spectroscopy. *J. Mater. Sci.* **2011,** *47* (3), 1522-1530.
(40) Gu, X.; Tian, S.; Zhou, Q.; Adkins, J.; Gu, Z.; Li, X.; Zheng, J., SERS detection of polycyclic aromatic hydrocarbons on a bowl-shaped silver cavity substrate. *RSC Adv.* **2013,** *3* (48), 25989-25996.
(41) Erdheim, G. R.; Birke, R. L.; Lombardi, J. R., Surface enhanced raman spectrum of pyrazine. Observation of forbidden lines at the electrode surface. *Chem. Phys. Lett.* **1980,** *69* (3), 495-498.
(42) Tackley, D. R.; Dent, G.; Ewen Smith, W., Phthalocyanines: structure and vibrations. *Phys. Chem. Chem. Phys.* **2001,** *3* (8), 1419-1426.
(43) Liu, Z.; Zhang, X.; Zhang, Y.; Jiang, J., Theoretical investigation of the molecular, electronic structures and vibrational spectra of a series of

first transition metal phthalocyanines. *Spectrochim. Acta A Mol. Biomol. Spectrosc.* **2007,** *67* (5), 1232-1246.
(44) Buimaga-Iarinca, L.; Morari, C., Translation of metal-phthalocyanines adsorbed on Au(111): from van der Waals interaction to strong electronic correlation. *Sci. Rep.* **2018,** *8* (1), 12728.
(45) Melendres, C. A.; Maroni, V. A., Raman spectra and normal coordinate analysis of the planar vibrations of iron phthalocyanine. *J. Raman Spectrosc.* **1984,** *15* (5), 319-326.
(46) Skúlason, E.; Bligaard, T.; Gudmundsdóttir, S.; Studt, F.; Rossmeisl, J.; Abild-Pedersen, F.; Vegge, T.; Jónsson, H.; Nørskov, J. K., A theoretical evaluation of possible transition metal electro-catalysts for N_2 reduction. *Phys. Chem. Chem. Phys.* **2012,** *14* (3), 1235-1245.
(47) Honkala, K.; Hellman, A.; Remediakis, I. N.; Logadottir, A.; Carlsson, A.; Dahl, S.; Christensen, C. H.; Nørskov, J. K., Ammonia synthesis from first-principles calculations. *Science* **2005,** *307* (5709), 555-558.
(48) Guo, X.; Gu, J.; Lin, S.; Zhang, S.; Chen, Z.; Huang, S., Tackling the activity and selectivity challenges of electrocatalysts toward the nitrogen reduction reaction via atomically dispersed biatom catalysts. *J. Am. Chem. Soc.* **2020,** *142* (12), 5709-5721.
(49) Cong, M.; Chen, X.; Xia, K.; Ding, X.; Zhang, L.; Jin, Y.; Gao, Y.; Zhang, L., Selective nitrogen reduction to ammonia on iron porphyrin-based single-site metal–organic frameworks. *J. Mater. Chem. A,* **2021,** *9* (8), 4673-4678.

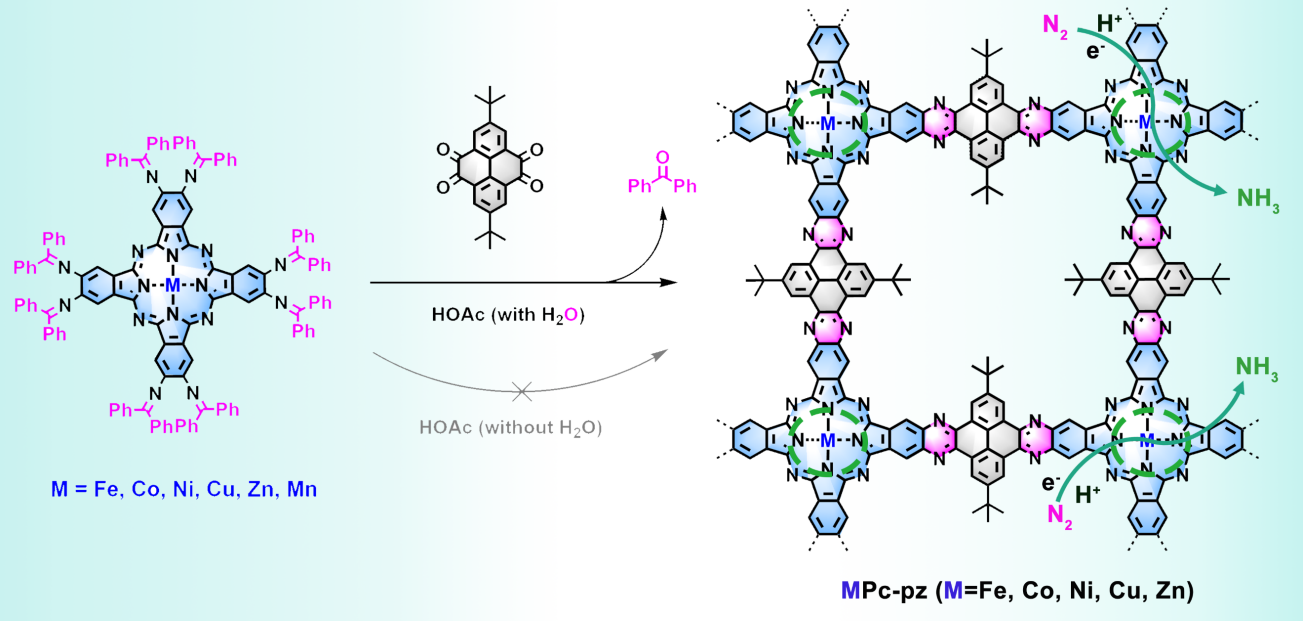

SYNOPSIS TOC

Two-dimensional conjugated covalent organic frameworks (2D c-COFs) immobilized with M-N_4-C centers, comprising metal-phthalocyanine (M = Fe, Co, Ni, Mn, Zn and Cu) and pyrene building blocks bonded by pyrazine linkages was developed as novel, defined and effective catalysts toward a simultaneous enhancement in the activity and selectivity of electrochemical NRR to yield ammonia.